Practical Papers, Articles and Application Notes

Flavio Canavero, Technical Editor

Both articles of the current issue are related to measurement techniques for EMC.

The first article is entitled "Shielded Cables Transfer Impedance Measurement" by Bernard Démoulin and Lamine Koné, with the TELICE Lab at the University of Lille, France. The determination of transfer impedance of cables and connectors is a common practice for several EMC applications, but it has various hidden subtleties that can often make the result of measurements inaccurate. Despite this fact, I don't remember having seen fresh and innovative discussions on this subject at conferences or in journal papers, recently. This article brings us the highly competent view of an experienced team on transfer impedance characterization of cables. In particular, Professor Démoulin played a significant role during the1970s at the former Laboratory for Radiopropagation and Electronics (now TELICE), where testing procedures for cable shielding effectiveness were developed and subsequently incorporated by IEC Standards. Recently, Professor Démoulin retired and now he enjoys writing books where he consolidates the long and rich experience on EMC he accumulated in his long carrier. I am delighted to have the privilege of offering you this article (and two more, that will appear in the next issues) shedding light on practical and more subtle fundamental issues of shielded cable transfer impedance measurements. I'm sure it will stimulate discussions and thoughts.

The second article is entitled "EMI Failure Analysis Techniques: III. Correlation Analysis" by Weifeng Pan and David Pommerenke from the EMC Lab of the Missouri University of Science and Technology in Rolla, Missouri. This is the third and last contribution of a series covering different methods for EMI failure analysis of devices. This paper focuses on how to determine the inter-relation between multiple near-field signals and the far-field signal, by means of correlation techniques. However, the reader must be warned that correlation analysis requires advanced measurements and data analysis methods and it is not meant to provide an immediate result for quick EMI troubleshooting.

In conclusion, I encourage (as always) all readers to actively contribute to this column, either by submitting manuscripts they deem appropriate, or by nominating other authors having something exciting to share with the Community. I will follow all suggestions, and with the help of independent reviewers, I really hope to be able to provide a great variety of enjoyable and instructive papers. Please communicate with me, preferably by email at canavero@ieee.org.

Shielded Cables Transfer Impedance Measurement

B. Démoulin, L. Koné
TELICE-IEMN Group, Université Lille 1 (France)

Introduction

Transfer impedance measurement represents perhaps the most objective methodology to estimate the shielding effectiveness of cables or connectors. Similarly to the propagation parameters of cables (ie, the characteristic impedance, the propagation velocity and the per-unit-length attenuation), the transfer impedance characterizes the shielding properties, independently of the external conditions of cables or connectors.

This article is devoted to the description of some measurement techniques that are commonly employed for transfer impedance determination [1], [2].

The first Section concerns the definition of transfer impedance as derived by means of a measurement setup including an injection line made by an outer metallic tube, coaxial with the shielded cable under test. The measurement procedure consists in generating along the shield a perturbing sinusoidal current, with ideally uniform longitudinal distribution. We will designate this setup as "triaxial" due to the existence of three coaxial cylinders, i.e., the outer tube, the shield under test and the inner conductor of the cable. For a cable with two wires inside the shield, such conductors must be shortened at their ends, in order to be equivalent to the single inner conductor of a conventional coaxial cable.

The second Section describes the coupling between the injection line and the coaxial cable, assuming that each line is matched, i.e. terminated with their respective characteristic impedances. This analysis will result in two equations providing the voltages generated at the coax terminations. Such voltages will be called near-end and far-end voltages. A detailed study of these equations will provide an insight about the role of propagation on the signal transfer and this, in turn, will allow us to derive rules for the reduction of systematic errors due to interference of signals propagating along the cable.

The third Section deals entirely with the technological description of triaxial setups, and provides tips for the estimation of the injection current and for the measurement of the very low voltages that must be collected at the terminations of the sample under test.

The fourth Section discusses the calibration of the measurement setup and describes the test samples needed to perform the calibration.

The fifth Section provides examples of measurements performed on coaxial cables of various types. One experiment clearly evidences the presence of the propagation phenomena encountered during the transfer impedance measurement of a cable with a length of approximately 10 m. Other results allow to appreciate the wide dynamic range related to transfer impedance measurements.

Definition of Transfer Impedance

Let us consider the coaxial cable shown in Fig. 1. A uniform current I_S, independent from the longitudinal variable z, flows along the shield. The internal conductor is connected to the shield at the extremity situated in $z = L_0$, while the extremity situated on the reference origin is connected with an impedance of value Z_0. Consequently, the residual voltage due to the shield imperfection assumes the value $V_c(0)$. We assume a sinusoidal current giving rise to a TEM mode, whose wavelenght is much larger than the cable length.

Assuming that Z_0 is approximately equal to the characteristic cable impedance Z_c, we can derive the simplified equivalent circuit of the cable, as represented in Fig. 2.

The electromotive source E_0 appearing in the diagram of Fig. 2 is given by $E_0 = Z_t I_{S0} L_0$, where I_{S0} is the constant value assumed by the current along the shield.

In principle, the transfer impedance can be experimentally determined by a current-to-voltage ratio, as follows

$$Z_t = \frac{1}{L_0}\frac{V_c(0)}{I_{S0}} \tag{1}$$

Different procedures have been considered to carry out the measurement of the transfer impedance of a shielded cable. First of all, we will analyze the most rudimental setup called "*Triaxial matched setup*".

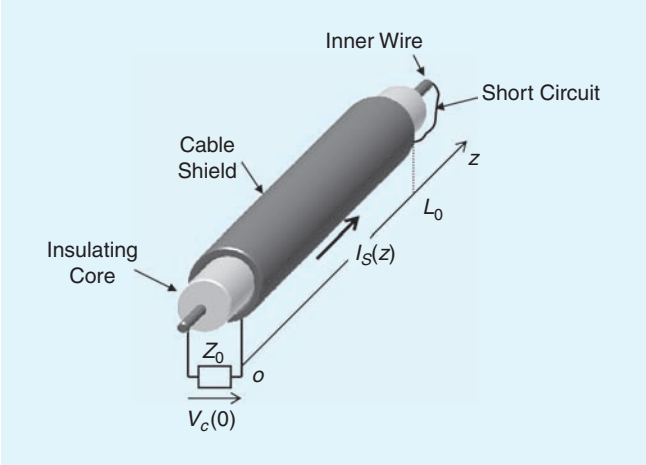

Fig. 1. The shielded cable and its terminations.

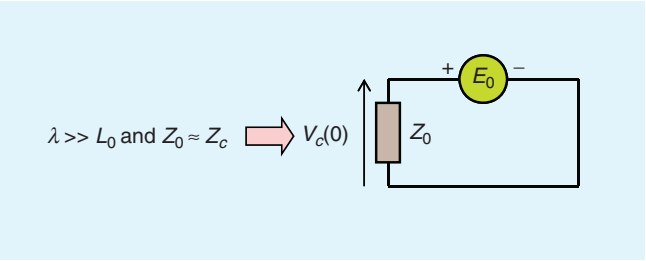

Fig. 2. Parameters of the equivalent circuit.

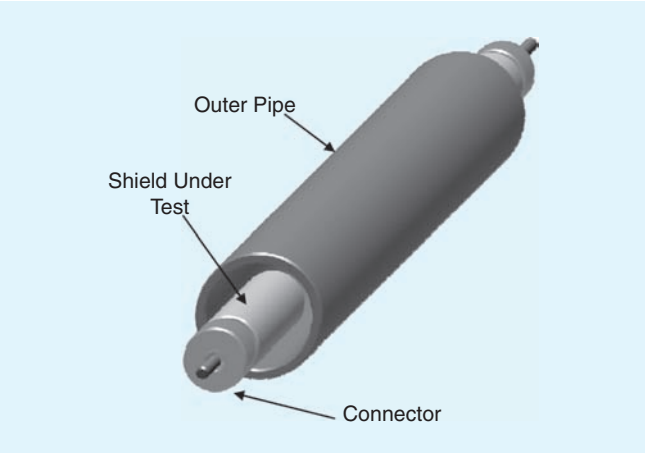

Fig. 3. Main elements of the triaxial setup.

Triaxial Matched Setup

The triaxial setup is constituted by a cylindrical pipe concentric to the cable shielding; this pipe forms a coaxial transmission line that canalizes the injected current required for the measurement. Fig. 3 shows a perspective view of the triaxial setup.

The longitudinal section of the above figure shows that this system is equivalent to a two-coupled transmission line system. Line 1 or "perturbing line", is made up of the external pipe and the cable shield under test. Line 2 consists of the cable under test coupled with the perturbing line by means of the transfer impedance. Lines 1 and 2 are represented by the following pairs of impedance and propagation constant: (Z_{c1}, γ_1) and (Z_{c2}, γ_2).

The configuration of Fig. 4 shows the measurement setup of the triaxial method, where both lines are matched. The crosstalk voltages produced at the near and far terminations are expressed by

$$V_c(0) = \frac{1}{2} Z_t I_{S0} \frac{1 - e^{-(\gamma_1+\gamma_2)L_0}}{\gamma_1 + \gamma_2} \tag{2}$$

$$V_c(L_0) = -\frac{1}{2} Z_t I_{S0} \frac{1 - e^{-(\gamma_1-\gamma_2)L_0}}{\gamma_1 - \gamma_2} e^{-\gamma_2 L_0} \tag{3}$$

The configuration of Fig.4, with line (2) matched at both ends, has the advantage of reducing systematic errors generated by propagation phenomena. For an analytical demonstration of this fact, we neglect conductors losses. Thus propagation constants γ_1 and γ_2 reduce themselves to completely imaginary quantities, which we will express as

$$\gamma_1 = j\frac{\omega}{v_1} \qquad \gamma_2 = j\frac{\omega}{v_2} \tag{4}$$

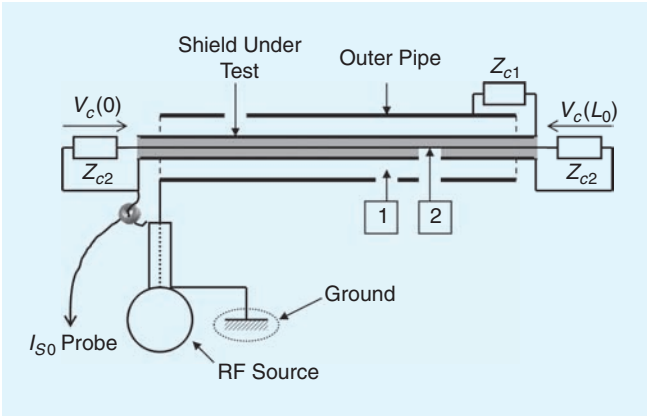

Fig. 4. Configuration of the triaxial setup for the measurement.

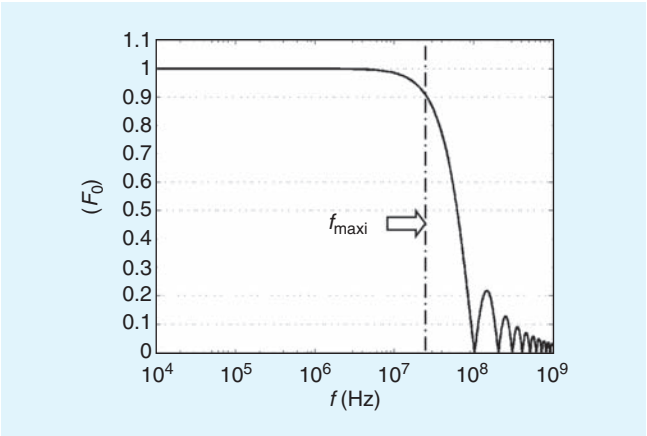

Fig. 5. Influence of propagation effects on the voltage $V_c(0)$.

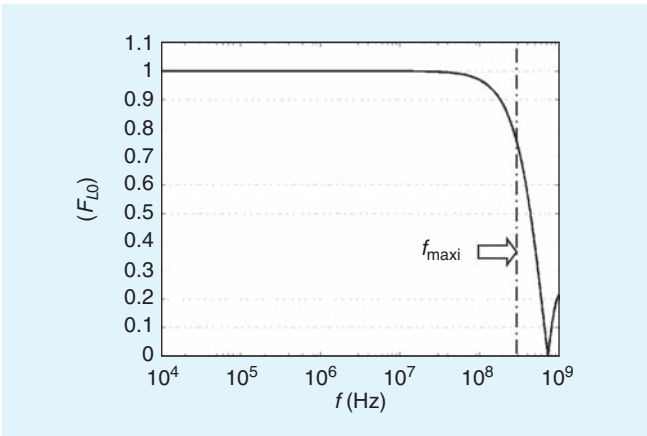

Fig. 6. Influence of propagation effects on the voltage $V_c(L_0)$.

In the above equation, v_1 and v_2 represent the propagation velocity of every line; these parameters, although not rigorously equal, usually have close values. In the low-frequency approximation, the phase angles contained in (2) and (3) are in absolute value much lower than unity, i.e., $|\gamma_1 L_0|$, $|\gamma_2 L_0| \ll 1$. Therefore we can adopt a truncated series representation of the exponential function, and the termination voltages are given by the following simplified expressions

$$[V_c(0)]_{LF} \cong \frac{1}{2} Z_t I_{S0} L_0 \tag{5}$$

$$[V_c(L_0)]_{LF} \cong -\frac{1}{2} Z_t I_{S0} L_0 \tag{6}$$

For high frequencies, the end voltages consist in the product between simplified equations (5) or (6) and a correction function dependent on propagation phenomena. Hence,

$$V_c(0) = [V_c(0)]_{LF} F_0(\omega, L_0) \tag{7}$$

$$V_c(L_0) = [V_c(L_0)]_{LF} F_{L0}(\omega, L_0) \tag{8}$$

where the correction functions F_0 and F_{L0} assume the following expressions:

$$F_0(\omega, L_0) = \frac{1 - e^{-j\omega\left(\frac{1}{v_1}+\frac{1}{v_2}\right)L_0}}{\left(\frac{1}{v_1}+\frac{1}{v_2}\right)L_0} \tag{9}$$

$$F_{L0}(\omega, L_0) = \frac{1 - e^{-j\omega\left(\frac{1}{v_1}-\frac{1}{v_2}\right)L_0}}{\left(\frac{1}{v_1}-\frac{1}{v_2}\right)L_0} e^{-j\omega\frac{L_0}{v_2}} \tag{10}$$

The following numerical example illustrates the behavior of correction functions. Let us consider that the triaxial bench length is $L_0 = 1$ m, and that the propagation velocities in the two coaxial waveguides are $v_1 = 0.8c$, $v_2 = 0.6c$ (c is the speed of light in vacuum). The curves represented in Figs 5 and 6 respectively show the evolutions of $F_0(\omega, L_0)$ and $F_{L0}(\omega, L_0)$, in a frequency band between 10 kHz and 1 GHz. Each graph contains a dashed vertical line crossing the curve at the value of 0.9. The frequency identified by this vertical line indicates the limit above which the error introduced by propagation phenomena is larger than 10 %. Consequently, this vertical line defines the maximum usable frequency for the triaxial bench. Also, this example shows that the limit for near-end crosstalk voltage measurements is around 30 MHz, while such limit moves to around 200 MHz for far-end crosstalk voltage measurements.

These figures show that, in order to reach high frequencies, it is preferable to measure far-end crosstalk voltage.

In the following section, we will examine some triaxial bench adjustments generally adopted to reduce measurement inaccuracies or to improve sensitivity.

Various Triaxial Setup Configurations

Injected Current Measurement

Fig. 7 shows three different toroidal transformers configurations that are commonly adopted to measure the current I_{S0} injected into the shielded cable under test. A discussion of the advantages and drawbacks of every solution follows.

In layout (a), the current probe is placed on the conductor connecting the RF generator and the external pipe. With this configuration, the measured current I_M is given by the vector sum of the current I_{S0} circulating into the shield and a leakage current I_R, representing the external pipe radiation (the

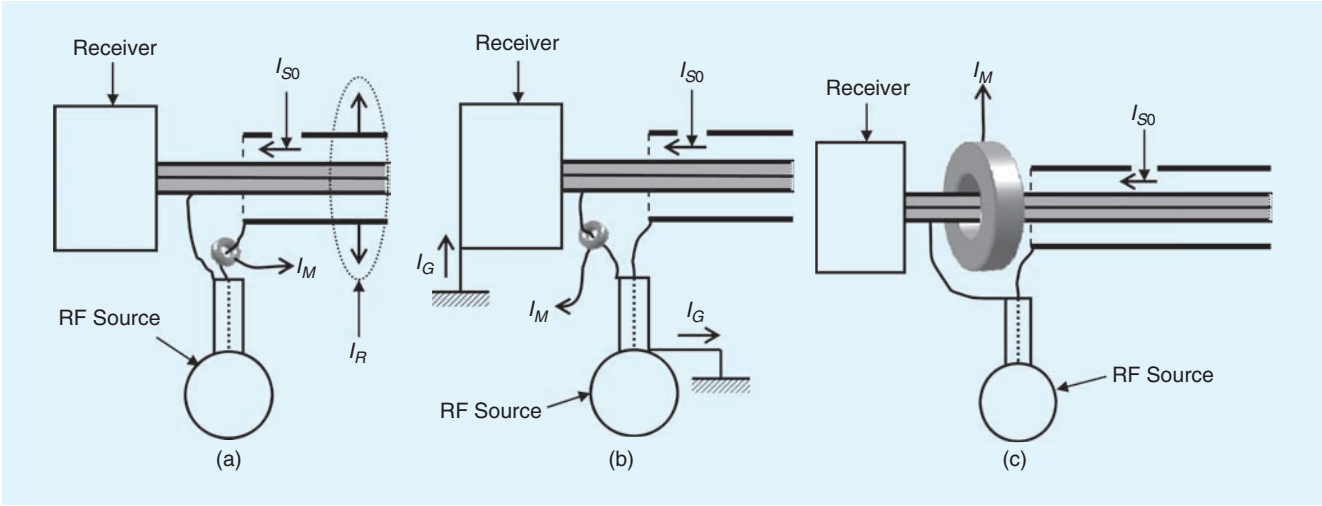

Fig. 7. Different configurations for the measurement of I_{S0}.

amplitude of I_R is generally lower than the current injected into the shield); in summary,

$$I_M = I_{S0} + I_R \tag{11}$$

The error introduced by this additional leakage current is often increasing at high frequencies or when resonances are happening on the pipe external conduit.

In layout **(b)**, the current transformer is placed on the conductor connecting the high-frequency ground connection of the source with the cable shield. With this second topology, the evaluated current is given by the sum of the current circulating into the shield and a leakage current I_G coming from the ground plane shared by the two connected instruments, that is:

$$I_M = I_{S0} + I_G \tag{12}$$

Generally, the current I_G has a lower amplitude than current I_{S0}, and their relative contribution depends on ground impedance circuits. For low frequencies under 10 kHz, the ground impedance is low, hence I_G contribution becomes significant. The effect of this phenomenon involves inaccurate determination of I_{S0}. For frequecies higher than 10 kHz, this error is negligible.

Layout **(c)** uses a toroidal transformer directly placed on the cable shield. Theoretically, only this configuration can give us the actual value of the current injected in the shield, i.e.

$$I_M = I_{S0} \tag{13}$$

Contrary to previous configurations, the installation of the transformer on the shield needs a more extensive magnetic circuit as regards to the probes previously used.

Voltage Measurement at the Termination of the Sample Under Test

In order to perform this measurement, several procedures are possible. The setup suggested in Fig. 4 does not allow for a great sensitivity; this configuration reduces the measurement amplitude dynamics below 100 $\mu\Omega$/m. The loss of sensitivity comes from the electromagnetic coupling between the external pipe and the receiver, as shown in Fig. 8. We may say that this

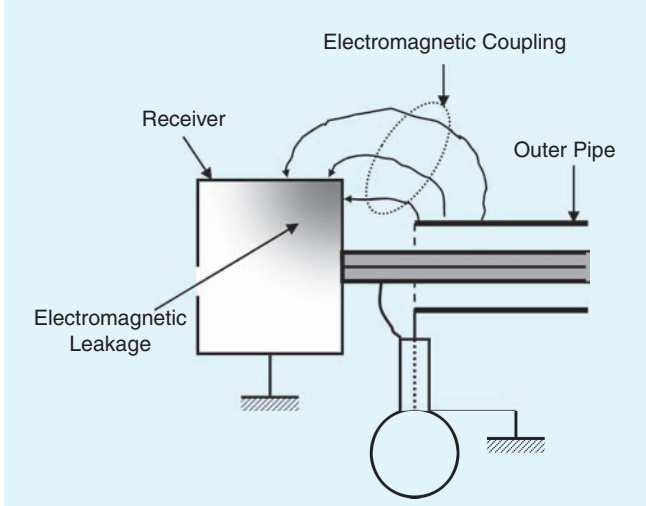

Fig. 8. Illustration of the undesirable coupling between the outer tube and the receiver.

parasitic coupling produces a current induction on the metallic structure of the receiver, whose electromagnetic radiation is captured by the internal circuits processing the low amplitude voltage detected on the test pipe termination. A second coupling path, not mentioned in the figure, comes from parasitic conduction on the receiver cables (e.g., the power cable or the multiwire bus linking the measurement unit with the monitoring computer). In order to reduce the effects of undesired electromagnetic coupling, the receiver must be protected by a shield connected according to the diagram in Fig. 9.

With this layout, the termination of the cable under test is connected to the receiver by means of a highly shielded connector placed on the metallic wall of the shielded cage. The transfer impedance must be weak enough to allow the residual voltage due to the ground current I_G to be much lower than the voltage that we intend to measure.

The power supply of the receiver placed in the cage can be battery-operated, or fed from mains through a lowpass filter placed outside the metal shield enclosing the measurement setup. Digital data transmission from/to computer and receiver need to be transferred via an optical fiber link. In order

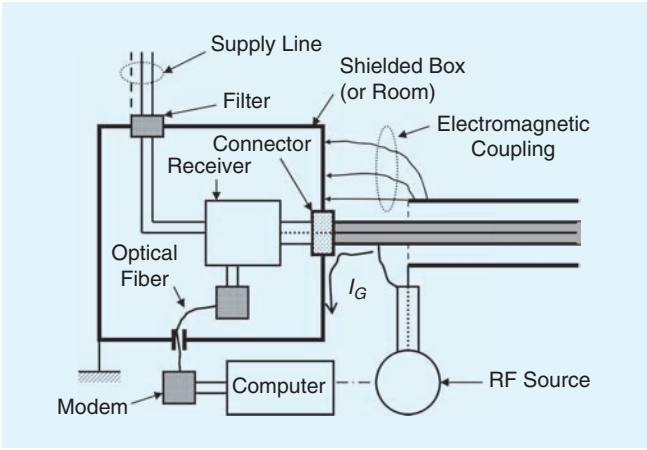

Fig. 9. Possible electromagnetic protections of the receiver.

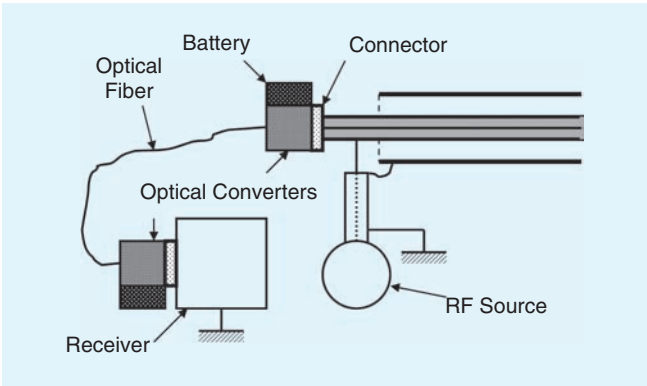

Fig. 10. Suppression of the parasitic electromagnetic coupling by the use of an optical transducer.

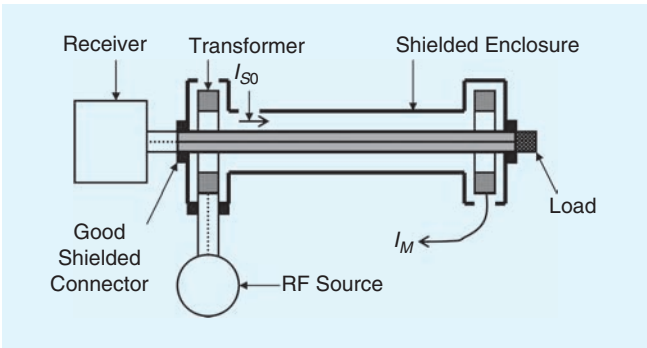

Fig. 11. Triaxial set up confined area by means of current transformers at both ends.

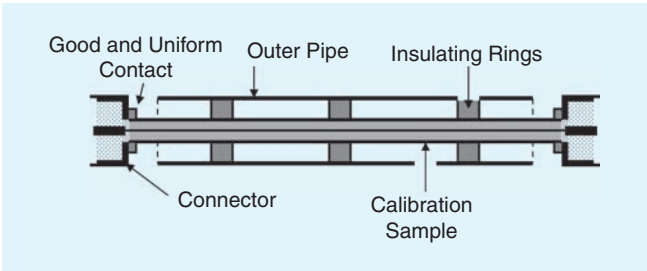

Fig. 12. Configuration used for the calibration of the triaxial setup.

to further improve measurement immunity, the voltage at the sample termination must be picked up when the current probe is disconnected from the Faraday cage. This precaution avoids a self-disturbance due to very low amplitude signals captured by the test tube.

Other solutions consist in bringing the external pipe to ground potential, in order to remove its own radiation. Fig. 10 shows a configuration where the contact points of the high-frequency source on the triaxial structure have been swapped. In this case, we avoid that the receiver ground network short circuits the source; the separation is done through an optical transducer, as shown in the figure.

To achieve the maximum electromagnetic immunity, transducers need to be equipped with autonomous power-supplies. Also, connectors with very low transfer impedance must be employed. After fulfillment of all these rules, triaxial setup sensitivity is only limited by the noise generated by the spectrum analyzer during signal amplification. This phenomenon can be reduced adopting a resolution bandwidth near or below 10 Hz.

With other topologies, we may reduce the external pipe radiation with an indirect current injection obtained by means of a magnetic coupler, which is a large-band high-frequency toroidal transformer. This device is shown in Fig. 11. With this configuration, the perturbing line must be short-circuited at both terminations; this function is accomplished by the external pipe. At the end of the perturbing line opposite to the emitting transformer, another transformer designed for the measurement of the induced current on the cable shield is located; hence $I_M = I_{S0}$.

The terminations of the cable under test are connected to the load impedance and to the receiver by highly shielded connectors. A narrow-bandwidth voltage amplifier inserted between the cable termination and the spectrum analyzer allows the transfer impedance evaluation with a sensitivity below the $\mu\Omega$/m (typically: $Z_t < 0.1\ \mu\Omega$/m). Contrary to the previously examined triaxial setup, the perturbing line of Fig.11, which ends with two short circuits, may enhance the influence of propagation phenomena and harm the measurements accuracy already above 10 MHz.

Transfer Impedance Measurement Setup and Calibration

The sample of the cable under test is centered in the external pipe by insulated spacers (see Fig. 12), and the external pipe diameter is set in order to have the perturbing line characteristic impedance ranging between 60 Ω and 40 Ω. The connections at the ends of the cable under test must make good contact with the outer side of the shield; a welded connection is recommended. The measurements quality highly depends on the care taken to mount the connectors.

The calibration of the transfer impedance measurement setup is performed by a test tube made up of a good conductor material (steel or copper). In fact, the advantage of having a homogeneus pipe reflects in an accurate prediction of the transfer impedance, whose expression is

$$Z_t = R_0 \frac{(1+j)\dfrac{E}{\delta}}{sh\left[(1+j)\dfrac{E}{\delta}\right]} \qquad (14)$$

where E is the pipe thickness, R_0 is the per unit length resistance and δ is the skin depth.

In the following numerical example, we study three different calibration samples with different thicknesses, in the frequency band between 10 kHz and 1 GHz, and with an amplitude dynamics from 10 mΩ/m to 0.01 $\mu\Omega$/m. Let us consider three samples with the same diameter $D = 12$ mm and thicknesses $E_1 = 0.5$ mm, $E_2 = 0.1$ mm, $E_3 = 0.05$ mm, made of copper (electrical conductivity $\sigma = 5.8 \cdot 10^7$ S/m). The plots of Fig. 13 show the transfer impedance frequency behavior of the three samples under consideration. The horizontal dotted lines indicate the sensitivity theresholds of the different measurements procedures: the line situated at 0.1 mΩ/m corresponds to the ordinary triaxial setup shown in Fig. 8; the line situated at 1.0 $\mu\Omega$/m shows the sensitivity of the sophisticated test benches shown in Figs 9, 10 and 11. Fig. 14 shows that the sensitivity threshold observed during calibration appears in the rising part of the characteristics.

The falling continuous line corresponds to the theoretical transfer impedance variation, as predicted by (14). The slope change starting at approximately 1.5 MHz is due to setup imperfections related to the transfer inductance of end connectors; the pure effect of this inductance is represented by the extrapolation shown by the oblique dotted line. According to this example, the parasitic transfer impedance is estimated to be $L_t \cong 0.2$ pH. Consequently, this imperfection limits the minimum measurable transfer impedance at $Z_{t\,min} \cong 2\ \mu\Omega$/m, and beyond this minimum, the sensitivity limit increases with frequency until it reaches 0.1 mΩ/m at 100 MHz. Above 100 MHz other limitations take over, due to amplitude variations generated by propagation mechanisms, as predicted by (9) and (10).

This example demonstrates that the realization of a sensitive measurement setup requires to mount high immunity connectors at the terminations.

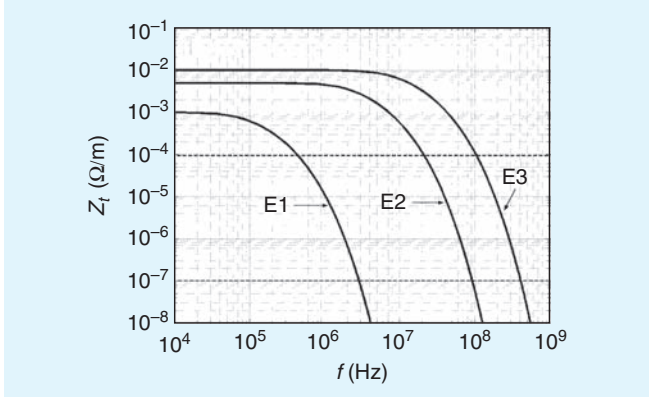

Fig. 13. Transfer impedance of the calibration sample as a function of frequency, for decreasing thicknesses E1, E2, E3 of the copper pipe.

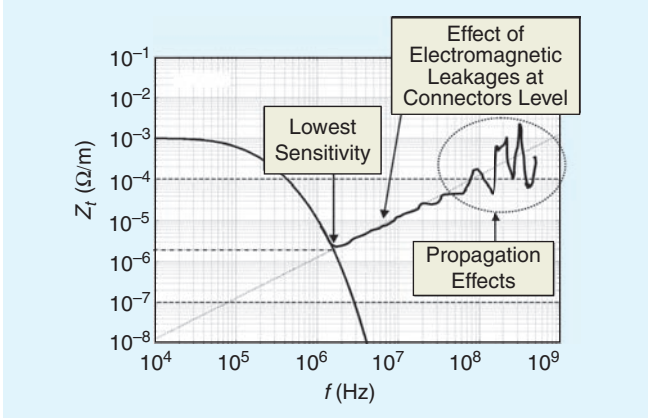

Fig. 14. Correlation of the transfer impedance curve for the calibration sample with the sensitivity threshold of measurements for the triaxial setup.

Examples of Transfer Impedance Measurements

Physical Illustration of Propagation Phenomena

The curves of Fig. 15 were obtained by means of the measurement procedure described in Fig. 10: the cable under test is a 10-m long braided coax of type KX-4, and the frequency range of the test is between 10 kHz and 100 MHz. This experiment has mainly an educational purpose, because it evidences the propagation phenomena expressed in (7) and (8), and the impact of the terms $F_0(\omega, L_0)$ and $F_{L0}(\omega, L_0)$ plotted in Figs. 5 and 6. From Fig. 15, we can observe that, below 1 MHz, the transfer impedance obtained as the ratio between voltage and current normalized by the length L_0 coincides with the transfer impedance of the cable. For the remainder of our reasoning, we assume that the transfer impedance of a braided cable [3] can be expressed as

$$Z_t = R_0 + j\omega L_t \qquad (15)$$

where R_0 is the per-unit-length resistance of the braiding and L_t is the transfer inductance, which comes from the magnetic coupling through the small apertures on the surface of the braided shield.

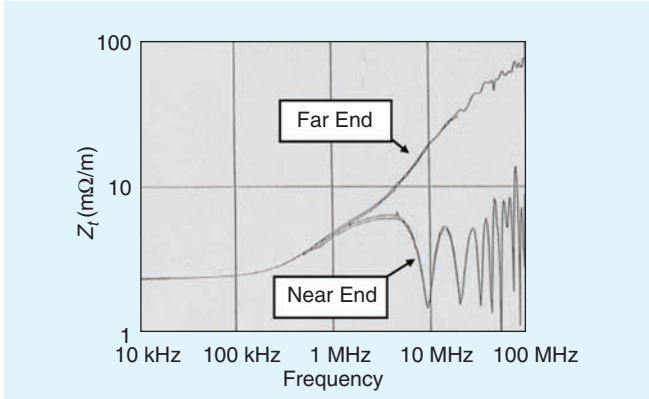

Fig. 15. Propagation phenomena affecting transfer impedance measurement in a 10-m long cable with single braid.

If we consider a measurement performed on a sample length on the order of 10 m, the influence of the propagation phenomena described by Figs. 5 and 6 should appear for frequencies in the vicinity of 2 MHz, if one measures the near-end voltage, and above 20 MHz for measurements of the far-end voltage. The experiment confirms very well the change of the behaviour vs frequency [4]; in fact, the curve produced by the near-end measurement shows a change of the slope above 2 MHz with alternate maxima and minima of the amplitude as predicted

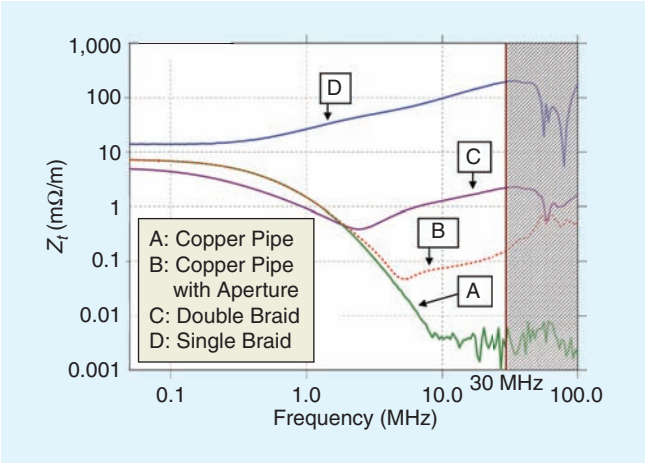

Fig. 16. Examples of transfer impedance measurements for cables A, B, C, D with different characteristics. The hatched area indicates the region influenced by propagation phenomena and by the noise level of the receiver.

by (9). According to the behaviour of the transfer function as predicted by eq. (15), the amplitude of maxima should be independent of frequency. In practice, the apparently random fluctuations of the level of maxima depends on the mismatch of the line injecting the current I_S in the shield. The mismatch is mainly due to parasitic inductance of the load and of the cable connecting the RF source to the injection line. As expected from (8) and (10), the use of far-end voltage seems more appropriate, since the slope of the curve remains unaltered up to 50 MHz.

Dynamic Range of Transfer Impedance

Fig. 16 collects four curves of transfer impedance of four cable samples with different physical structure. Measurements were done by means of a matched triaxial setup, according to the arrangement described in Fig. 9. The length of all cables under test was 1 m, hence the usable frequency range is below 30 MHz. Nevertheless, results are displayed up to 100 MHz, in order to point out the measurement artefacts due propagation effects. Hatching on the right-hand side of Fig. 16 indicates the unusable part of the graphs affected by propagation phenomena. The lowest frequency of measurement is located at 50 kHz, due to the current sensor low cut off. The dynamics of the vertical axis extends from 1 $\mu\Omega$/m to 1 Ω/m, i.e., 120 dB. The following subsections refer to each of the samples and provide a physical interpretation of the respective transfer impedance curves.

Sample A

This sample is a coaxial cable with a solid tubular copper shield with a diameter of 3.6 mm and a thickness of 250 μm. The transfer impedance model of (14) applies to this cable, and the the down trend of the curve reveals the contribution of skin effect behaviour predicted by Schelkunoff [5]. The lowest frequency (50 kHz) of the measurement is such that the penetration depth of the electric field is larger than the shield thickness, which determines a per-unit-length resistance of the shield approximately equal to 7 mΩ/m. From 200 kHz, the transfer impedance starts lowering down to a minimum value of 3 $\mu\Omega$/m at 8 MHz. We can conclude that the previous value represents the minimum sensitivity of the measurement setup, determined by the noise floor of the receiver, which in this case was a spectrum analyser.

Sample B

Sample B is identical to A, except that the operator has purposedly reduced the torque on the SMA connector at the terminations of the sample itself. This anomaly produces an increase of the transfer impedance, visible above the frequency of 2 MHz. In fact, the consequence of the torque reduction is a leakage of magnetic flux, as illustrated by Fig. 14.

Sample C

The cable under test in this case is the type RG214 with a shield made of two tinned copper braids in uniform contact along their length [6]. The increase of the shield cross-section results in a reduction of the per-unit-length resistance; moreover, the juxtaposition of the two braids produces a reduction of the total transfer inductance due to magnetic leakage through a large amount of uniformly distributed small apertures appearing at crossing points of the woven wires. The reason of decreasing values of the transfer impedance up a frequency of 3 MHz is then similar to the case of a homogeneous tubular shield. However, the change of slope of the curve above 3 MHz indicates that magnetic leakage becomes predominant. Between 30 and 100 MHz, the curve fluctuations must be related to propagation phenomena. A measurement of the far-end voltage allows us to move the upper frequency to 100 MHz.

Sample D

This sample is made by a coaxial cable with a simple braided shield, of type KX15 (RG58). The measurement shows a behaviour very similar to the model of (15). However, a careful look at the transfer impedance curve in the frequency range between 300 kHz and 10 MHz shows that the increase is proportional to the square root of the frequency, which is in contrast to the linear prediction of (15). This behaviour finds an explanation in electromagnetic coupling phenomena, as illustrated by previous work [7], [8]. Above 10 MHz, the curve changes again its shape, and tends to a linear behaviour, but—contrary to the result of (15)—implies a minus sign for the transfer inductance [9]. The choice of a negative sign is implied by the orientation of the magnetic leakage flux penetrating in the cable and depending on the braid pitch angle. It ought to be remarked that such behaviour is specially related to pitch angles lower than 30 deg, while in the other cases the transfer impedance follows rigorously the model of (15) with a positive transfer inductance.

Conclusion

Contrary to other measurements of electromagnetic compatibility, the determination of the transfer impedance of shielded cables and connectors provides in general a relative accuracy lower than 20%. This is certainly due to a calibration process using a sample made of a solid homogeneous tubular shield. In fact, the transfer impedance of a copper pipe monotonically decreases with frequency, and it is well adapted to detect the weaknesses of the measurement chain. The coupling region between the setup and the high-sensitivity receiver needed to

measure the voltage at the sample terminations is very often responsible for such weaknesses. On the other hand, the measurement reproducibility is independent both of the setup arrangement and of the acquisition chain, since the care in samples preparation and the operator skill play a significant role. Evidently, the practical manner by which terminal connectors carrying low-level signals are mounted on the sample, makes the difference. Hence, a good practice is to repeat the measurement for several installations of the sample in the setup, in order to appreciate the level of uncertainty.

As described in the fifth Section, propagation phenomena produce a systematic uncertainty, appearing when the dimension of the sample under test with respect to wavelength exceeds 10%. Using the far-end voltage measurement allows to shift this limitation by approximately a decade in frequency, i.e., towards an almost unitary ratio between the sample dimension and wavelength. However, only very specialized test setups allow to reduce more effectively the propagation effects.

It ought to be mentioned that the description of bench setup for the transfer impedance measurements is the object of an international standard released by IEC [10]. Moreover, the present article only mentions the measurement technique based on the injection of a sinusoidal current. Impulsive currents can also be adopted, with the advantage of a faster interpretation of results; in addition, by means of the Fourier Transform technique, the transfer impedance phase is readily extracted [7].

References

[1] L. Halme, B. Szentkuti "The Background for Electromagnetic Screening Measurements of Cylindrical Screens" Technische Mitteilungen PTT, 1988.

[2] C. Goldstein, P. Mani "CW and Pulsed Mode Transfer Impedance Measurements in Coaxial Cables" IEEE Transactions on Electromagnetic Compatibility, Vol. 34, N. 1, February 1992, pp 50–57.

[3] E. F. Vance "Shielding Effectiveness of Braided-Wire Shields", IEEE Transactions on Electromagnetic Compatibility, Vol. 17, N. 2, May 1975, pp 71–77.

[4] M. Rochdi "Etude Comparative des Méthodes de Mesure de l'Impédance de Transfert de Cables et Application au Développement d'un Testeur de Cordons Blindés utilisable sur une Chaine de Fabrication" PhD Thesis, Université de Lille, 1990.

[5] S. A. Schelkunoff, "The Electromagnetic Theory of Coaxial Transmission Lines and Cylindrical Shields", Bell System Tech., 1934, pp 533–579.

[6] E.P. Fowler "Superscreened Cables" Radio Electr. Eng. Vol 49, January 1979, p 32.

[7] B. Démoulin, P. Degauque, R. Gabillard "Transient Response of Braided-Wire Shields" IEEE, International Symposium on EMC, San Diego, USA, 1979 79CH1383-9 EMC, Symp. Record pp 19–26.

[8] B. Démoulin, P. Degauque, M. Cauterman "Shielding Effectiveness of Braids with High Optical Coverage" 4th International Symposium on EMC, Zurich, Switzerland, 1981 Symp. Record pp 491–495.

[9] P. J. Madle "Contact Resistance and Porpoising Effects in Braid Shielded" Proc. IEEE, Int. Symp. EMC, 1980, p 206.

[10] Standard : IEC 96-1, Radiofrequency Cables.

Biographies

Bernard Démoulin *was born in 1946. He received his Ph.D in 1981 and until 2008, was head of the EMC group at the IEMN-TELICE Laboratory. He is presently professor emeritus at the University of Lille, France. His domain of expertise is mainly related to the effect of electromagnetic coupling through cables, transfer impedance measurement and the study of Mode Stirred Reverberation Chambers. He is a senior member of the French society of electrical engineers (SEE) and an URSI correspondent member.*

Lamine Koné *was born in 1956, he received his Ph.D degree in 1989. Since 1990, he has been working as engineer in the IEMN-TELICE laboratory at the University of Lille, France. His domain of expertise deals with EMC measurements, especially concerning the transfer impedance on shielded cables or connectors and tests carried out in mode-stirred reverberation chambers.*

EMI Failure Analysis Techniques: III. Correlation Analysis

Weifeng Pan, Gang Feng, and David Pommerenke
EMC Laboratory, Missouri University of Science and Technology

Introduction

Locating the emission source can be the most challenging part in EMI failure analysis. In the second article [1], a measurement sequence for source identification in complex systems was recommended. A variety of methods can be used to find the correlation between the far-field and a near-field signal. The correlation can be a similarity either in frequency spectrum or in time domain, or in joint time-frequency spectrogram. When multiple near-field sources potentially cause the emission at the same frequency and the near-field spectra cannot be visually correlated to far-field sideband signature, a mathematical correlation analysis can be performed [2]. Some commercial systems are also available [3][4]. The correlation analysis is an advanced measurement and data analysis method, which requires complex hardware for multi-channel time-synchronized measurement and extensive post-processing of measured data. Therefore it is not meant to provide immediate result for quick EMI troubleshooting.

Mathematical Correlation Methods

The EUT used in this article to illustrate the methodology had broadband emission centered at 667 MHz (also discussed in Zero Span Measurement in [5]). This radiated emission frequency is one of harmonics of the clock and data signals. It is generated from several ICs and modules. Several suspected EMI sources and their coupling paths were located, e.g., ICs with a heat sink, high speed signal cable bundles and a USB connector.

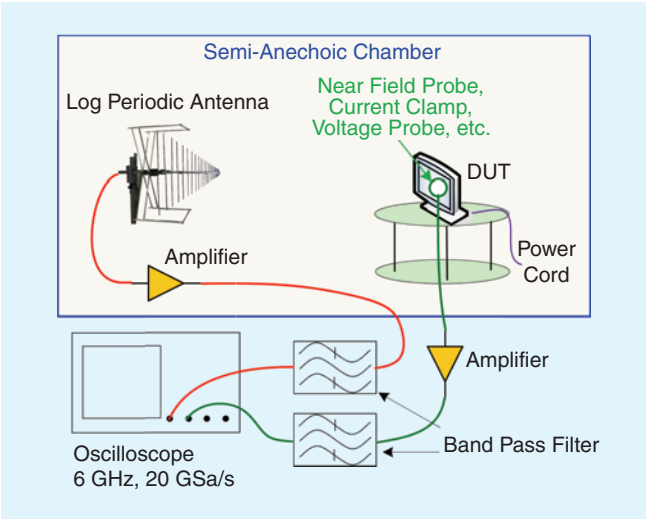

Fig. 1. Time-synchronized measurement of far-field and near-field for correlation analysis.

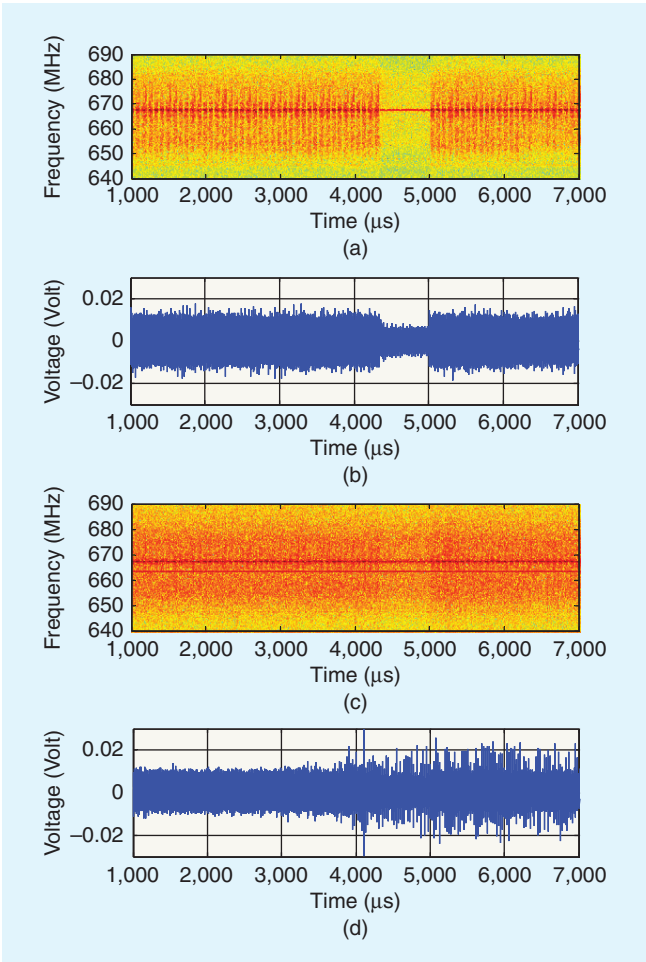

Fig. 2. STFFT spectrograms (1st and 3rd plots) and time domain waveforms (2nd and 4th plots) of near-field and far-field signals.

The correlation analysis requires time-synchronized measurement of the far-field and near-field signals. This can usually be implemented using multi-channels on an oscilloscope, as shown in Figure 1. The use of band pass filters is advised to attenuate signals that are not of interest and to achieve a better signal to noise ratio.

Depending on the local quantity, a variety of test accessories can be used. E-field or H-field probes are for measuring near field, current clamps for common mode current on cables, oscilloscope voltage probes for direct voltage measurement at a port defined between "grounds" or metal parts.

Listed in Table 1, there are several correlation analysis methods that have been in practice in our EMC lab. Some of them are introduced in this article.

STFFT Correlation

As introduced in the second article [1], the STFFT displays the spectral content of a signal in time domain. The correlation between the STFFT spectrograms of the near-field and far-field signal is a good indication of the likeliness of a near-field signal to be the EMI source. The STFFT result of a near-field signal and the far-field is shown in Figure 2. The near-field signal was the output from a current clamp around the high speed signal cable. The first and second plot show that the near-field signal is amplitude modulated by pulses of different width. Its spectrum is symmetrical. The far-field signal in the third and fourth plots is very noisy. It is a combination of three signals: an amplitude modulated signal similar to the near-field signal, a clock signal at 663.5 MHz, and a noise-resembling signal with a wide spread spectrum. There is a noticeable dropout of the near-field signal in the time waveform between 4300~5000 μs. However, the corresponding dropout in the far-field signal is overwhelmed by other signals and can barely be seen. The STFFT analysis indicates the measured near-field signal constitutes only a small fraction of the total radiated emission centered at 667 MHz. The correlation between this near-field signal and the far-field signal is weak. Other analysis techniques will be used to identify the correlation to this complicated far-field signal.

Envelope Correlation

As it has already been seen, amplitude modulated signals are very common in EMI problems. The envelope of the time domain amplitude is an important attribute of the amplitude modulated signals. Here the envelope is defined on a specified carrier frequency. It's the spectrum amplitude at that frequency versus time. After capturing the time domain data, their envelopes need to be determined. One way to do so is to extract the envelope from the amplitude data of the STFFT spectrogram at the carrier frequency, i.e., to plot one row of data in the STFFT spectrogram. This can also be achieved by using zero span measurement on a spectrum analyzer. However, if the envelope changes randomly, time-synchronized measurement of two channels is necessary, which cannot be done on most spectrum analyzers.

Cross-correlation function can be used to compare the envelopes of two signals. The cross-correlation of two discrete signal sequences is defined as:

$$R_{xy}(m) = E\{x_{n+m}\, y_n^*\} = E\{x_n\, y_{n-m}^*\} \qquad (1)$$

where x and y are jointly stationary random processes and $E\{\}$ is the expected value operator. R_{xy} is zero when x and y are uncorrelated. If the two processes are correlated, R_{xy} will reach its maximum when m is equal to the time difference between

TABLE 1. OVERVIEW OF THE CORRELATION METHODS.

Correlation Method	Brief description
short-term Fast Fourier Transform (STFFT)	Correlate the time changes of the spectral composition.
Direct correlation	Determine the correlation coefficient between two time vectors.
Envelope correlation	Determine the signal's envelope first and then analyze the correlation between the time changing envelopes.
Amplitude density distribution	Compare the amplitude density distribution of near-field and far-field signals.
Sideband analysis	Compare phase noise or sideband of signals in the near-field to the far-field signal.
Timing analysis	Compare the timing of events in the near-field to timing observed in the far-field signal.

the two processes. In practice, only a finite segment of the infinite long random process is available. The cross-correlation [6] of two discrete signal segments, x and y, each with a length of N is defined as:

$$\hat{R}_{xy}(m) = \begin{cases} \sum_{n=0}^{N-m-1} x_{n+m} y_n^* & 0 \le m \le N-1 \\ \hat{R}_{xy}^*(-m) & 1-N \le m < 0 \end{cases} \quad (2)$$

Extract the envelopes at 667 MHz from the far-field and a near-field signal, as shown in Figure 3. They are both amplitude modulated by periodical signals. The correlation function in the bottom plot indicates that the two envelopes have the same periodicity of about 15 µs. This confirms that this near-field signal and the far-field signal are amplitude modulated by one same signal.

Time synchronization gives timing information between signals. In this case, although the cross-correlation appears to be periodic, the offset of the peak position from zero shows the lead or lag of one signal to the other. This can help find the most relevant near-field signal among others, as demonstrated in Direct Correlation.

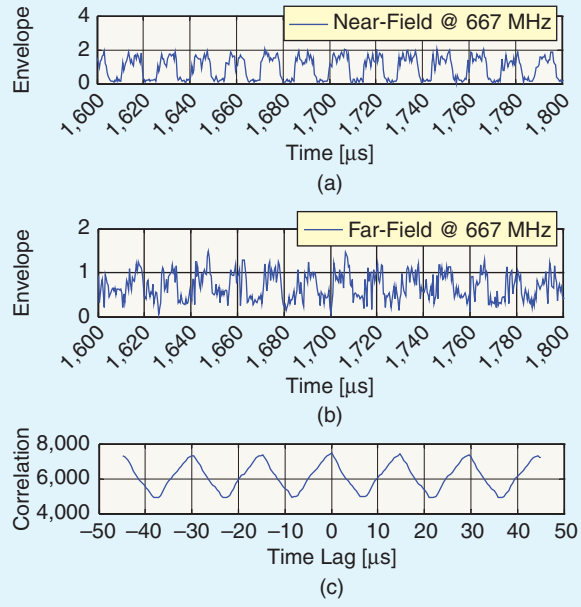

Fig. 3. Envelope at 667 MHz of a near-field signal (top) and the far-field (middle). Bottom: the cross-correlation of these two signals.

Coherence Factor

A more direct way to find the relation between two signals is to calculate the coherence factor of their frequency spectra. The coherence factor [7] is defined as:

$$C_{xy}(f) = \frac{|P_{xy}(f)|}{\sqrt{P_{xx}(f)P_{yy}(f)}} \quad (3)$$

where P_{xy} is the cross power spectral density of sequences x and y; P_{xx} and P_{yy} are the power spectral density of sequence x and y respectively. Coherence factor is a function of frequency, with a value between 0 and 1. If two signals are linearly related, the coherence factor will be "1" at any frequency. A coherence factor of "0" indicates that two signals are not related at that frequency.

The result of coherence factor analysis is shown in Figure 4. The Y axis is in log scale. Because band-pass filters centered at 667 MHz were used in these measurements, the peaks outside the pass-band are a result of random noise. A fairly strong coherence can be observed in the narrow frequency band around 667 MHz. While a quantitative threshold for determining coherence is difficult to define, a coherence factor between 0.8 and 1 usually indicates a good correlation. But more important is the relative value between near-field data measured at different locations of suspected EMI sources. The coherence factor can be used to determine which near-field signal best correlates to the far-field signal.

Direct Correlation

Direct correlation is to do a cross-correlation calculation between two time-synchronized waveforms. Figure 5 shows the

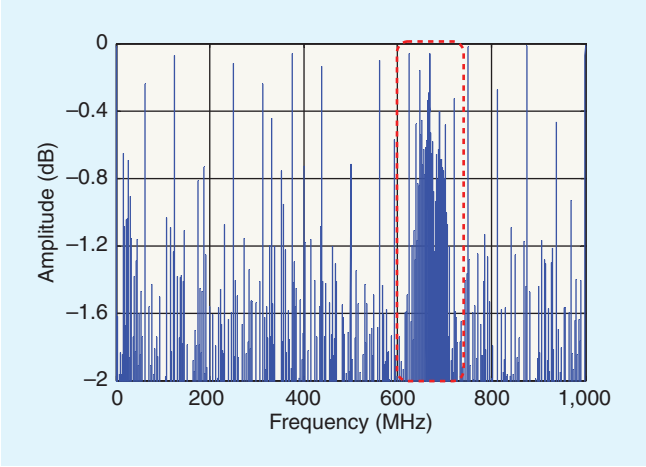

Fig. 4. Coherence factor between a near-field signal and the far-field signal.

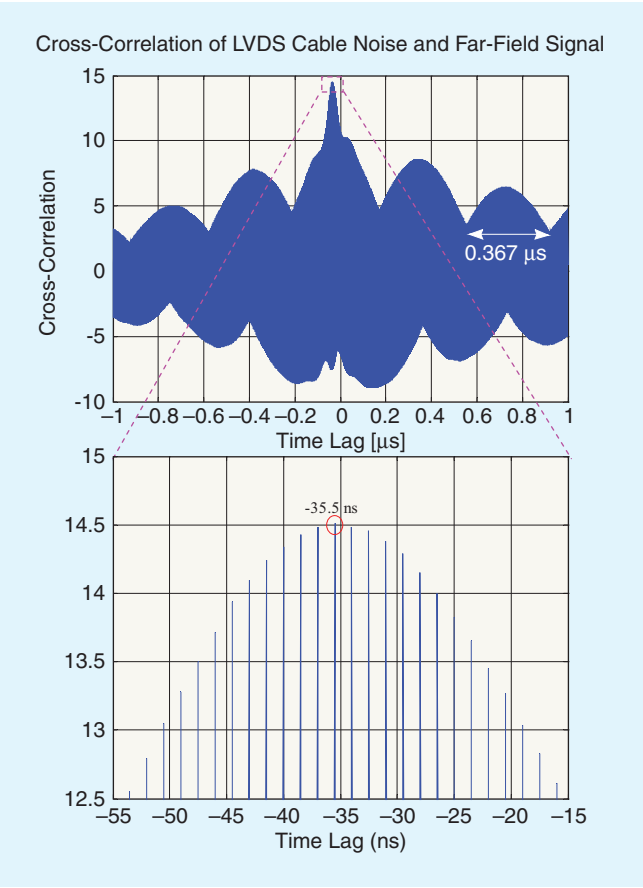

Fig. 5. Direct correlation of a near-field signal and the far-field.

direct correlation between a near-field signal and the far-field. The maximum peak is at −35.5 ns, which suggests the near-field leads 35.5 ns to the far-field. The delay is caused by different signal paths of the near and far-field measurement, which include cables, distance to antenna, and devices such as filters and amplifiers. In the case where several near-field signals are found to be correlated to the far-field, the signal which precedes all others in time has the best chance to be the EMI source.

The separation between the peaks in the bottom plot of Figure 5 is about 15 ns, corresponding to the main signal at

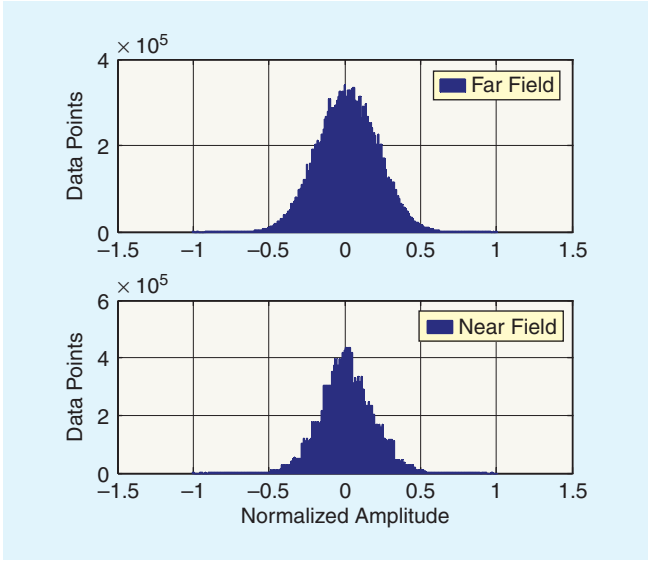

Fig. 6. Comparing the amplitude density distribution of far-field and a near-field signal. Both have Gaussian-shaped distributions.

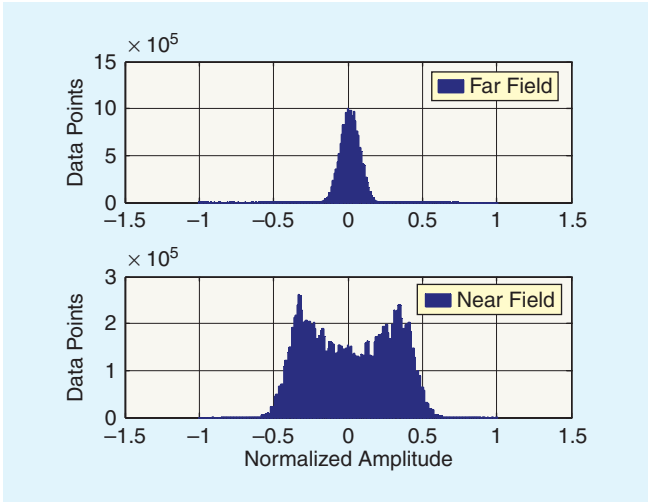

Fig. 7. Amplitude density distribution of the far-field and from a signal captured by current clamp.

667 MHz in both near and far-field. The envelope of the cross-correlation also has a repetition of 0.367 µs, corresponding to the 2.7 MHz amplitude modulating signal in both near and far-field. In summary, the direct cross-correlation of two time domain waveforms effectively reveals the delay and periodicity information of two correlated signals.

Amplitude Density Distribution

The amplitude density distribution shows the probability for the amplitude of a time domain waveform to occur at a certain value. In general, two well correlated signals should have the similar amplitude density distribution. Exceptions to this can occur in non-linear systems, where the input and output signals can have similar spectral information, but totally different amplitude distributions. Further, one cannot remind often enough that correlation is not a measure for causality. Two similar amplitude distributions do not necessarily mean two

signals are well correlated. It requires further information to show causality. In our experience the amplitude density distribution turns out to be useful for excluding causality.

The amplitude distribution comparison between the far-field signal and a near-field signal in Figure 6 shows a good similarity. Both are somewhat Gaussian-shaped. Of course, it should be ensured that the time domain data has sufficiently good signal to noise ratio. Otherwise the amplitude density distribution of the noise, which is also Gaussian-shaped, would dominate.

In another case presented in Figure 7, the amplitude density distribution of a near-field signal is very different to that of the far-field signal. This indicates that the emission from this source contributes very little, if any, to the far-field.

Conclusion

Correlation analysis is an important step in the recommended measurement sequence [1] for EMI source identification. It helps determine the inter-relation between multiple near-field signals and the far-field signal. This paper introduced five essential mathematical correlation analysis techniques for identifying EMI source and coupling path. When applicable, multiple correlation techniques should be used to reveal more information of the correlation between the signals.

References

[1] Weifeng Pan and Pommerenke, D., "EMI Failure Analysis Techniques: II. Joint Time-Frequency Analysis," IEEE EMC Society Newsletters, Summer 2009 – Issue No. 226.

[2] Gang Feng, Wei Wu, Pommerenke, D., Jun Fan, Beetner, D.G., "Time synchronized near-field and far-field for EMI source identification," IEEE International Symposium on Electromagnetic Compatibility, 2008.

[3] http://www.sara.com/EM/cassper/index.html, CASSPER system, SARA, Inc. May 2010.

[4] Parhami, P., Marino, M., Watkins, S., Nakauchi, E., "Innovative pre-compliance test methodology using ambient cancellation and coherence detection techniques," IEEE International Symposium on Electromagnetic Compatibility, 1999, vol.2.

[5] Weifeng Pan and Pommerenke, D., "EMI Failure Analysis Techniques: I. Frequency Spectrum Analysis," IEEE EMC Society Newsletters, Fall 2009 – Issue No. 223

[6] Orfanidis, S.J., "Optimum Signal Processing. An Introduction," 2nd Edition, Prentice-Hall, Englewood Cliffs, NJ, 1996.

[7] "mscohere", magnitude squared coherence, Matlab Product Help, 1984–2008 The MathWorks, Inc.

Biographies

Weifeng Pan *is currently an EMC design engineer at Google Inc., in Mountain View, California. He received the PhD degree in 2009 from the Electromagnetic Compatibility Lab at the Missouri University of Science and Technology. In 2008, he was an intern at IBM, Research Triangle Park, North Carolina. He worked as an RF design engineer at UTStarcom (China) from 2002 to 2005. He received the BSEE degree in 1999 and the MSEE degree in 2002 from Tsinghua University, in Beijing, China. His interests include electromagnetics, EMC and signal integrity.*

David Pommerenke *received the Ph.D. degree from the Technical University Berlin, Germany in 1996. After working at Hewlett Packard for five years, he joined the Electromagnetic Compatibility Lab at the University of Missouri-Rolla (now Missouri S&T) in 2001 where he is currently a tenured professor. He has published more than 100 papers and is an inventor on nine patents. In addition to other professional activities, he is the US representative of the ESD standard working group within the IEC TC77b. He is a past Distinguished Lecturer for the IEEE EMC Society (2006–2007). His research interests include system level ESD, numerical simulations, EMC measurement methods, and instrumentations.* **EMC**